Magnetic structures in the quadrupolar compound $TmAu_2$

2001 J. Phys.: Condens. Matter 13 929

(http://iopscience.iop.org/0953-8984/13/5/312)

INSTITUTE OF PHYSICS PUBLISHING JOURNAL OF PHYSICS: CONDENSED MATTER

J. Phys.: Condens. Matter **13** (2001) 929–943 www.iop.org/Journals/cm PII: S0953-8984(01)18782-5

Magnetic structures in the quadrupolar compound $TmAu_2$

M Amara[1,4], P Morin[1,5], P Burlet[2] and P Lejay[3]

[1,6] Laboratoire Louis-Néel, CNRS, BP 166X, 38042 Grenoble-cédex, France
[2] Magnétisme et Diffraction Neutronique, DRF/MC. Centre d'Etudes Nucléaires BP 85X, 38041 Grenoble-cédex, France
[3,6] CRTBT CNRS, BP 166X, 38042 Grenoble-cédex, France

E-mail: amara@polycnrs-gre.fr

Received 7 November 2000, in final form 4 January 2001

Abstract

The occurrence of a quadrupolar ordering within the γ orthorhombic symmetry at 7 K in $TmAu_2$ ($MoSi_2$-type tetragonal structure) was recently discovered. The existence of an antiferromagnetic ordering around 3 K in the quadrupolar phase leads to complex magnetic phase diagrams in the (H, T) plane. From neutron diffraction studies on a single crystal, a magnetic structure is determined for each of the five phases observed for a magnetic field applied along the twofold orthorhombic axis. The complexity of the phase diagram can be understood as the result of a conflict, under field, between quadrupoles and antiferromagnetic moments, associated with a rather degenerated maximum for the $J(Q)$ Fourier transform of the exchange couplings. Then classical arrangements perpendicular to the field and Ising-type behaviours are observed; in the latter case, the incommensurate nature of the magnetic interactions leads to behaviours of devil's staircase type.

1. Introduction

The studies of magnetoelastic properties has soared in popularity in the seventies for insulating compounds. Rare-earth (R) orthophosphates and orthovanadates are now considered as archetypes of the cooperative Jahn–Teller effect [1]. Magnetoelastic couplings are also present in R intermetallics, large enough to compete with the magnetic interactions; this has made the development of microscopic models considering both types of interactions, quadrupolar and magnetic, in the presence of the crystalline electric field necessary [2]. Concerning quadrupolar couplings, the main feature is that in insulators, the magnetoelastic coupling clearly dominates the pair interactions and induces the Jahn–Teller transition, whereas in intermetallics, the

[4] Author to whom correspondence should be addressed.
[5] Deceased.
[6] Associated with the University Joseph-Fourier of Grenoble.

0953-8984/01/050929+15$30.00

quadrupolar ordering is driven by the indirect pair interactions, its best evidence being the symmetry lowering associated with the magnetoelastic coupling.

In rare-earth intermetallics, the existence of quadrupolar interactions has been thoroughly proved in the case of the cubic symmetry with record spontaneous magnetostriction (up to 1.7% for the tetragonal symmetry lowering mode) and with quadrupolar orderings observed in the paramagnetic state as in TmCd and TmZn. Rarer are similar analyses for lower symmetries owing to the large number of crystalline electric field (CEF), magnetoelastic and quadrupolar pair interactions coefficients to be determined. However, the tetragonal rare-earth intermetallic $TmAg_2$ was shown to undergo at $T_Q = 5$ K a second-order transition to a γ orthorhombic state, that is with a O_2^2 order parameter in the definitions of Stevens equivalent operators [3]. No magnetic ordering exists in $TmAg_2$ [4]. Recently, a similar quadrupolar ordering was observed at 7 K in the isomorphous compound $TmAu_2$, with very reminiscent properties [5,6]. In this system, an antiferromagnetic ordering occurs around 3 K in the orthorhombic phase. These two tetragonal compounds then constitute a set reminiscent of the cubic TmZn and TmCd one. In both TmCd and $TmAg_2$, the magnetic bilinear interactions are not large enough to induce a magnetic moment on the singlet ground state and the magnetic system remains undercritical in the ferroquadrupolar phase.

On the contrary, TmZn and $TmAu_2$ order ferro- and antiferromagnetically, respectively. In TmZn, both the magnetic and quadrupolar orderings are ruled by ($q = 0$) mechanisms at the centre of the Brillouin zone and the magnetic state is easy to understand [2]. Unlike TmZn, $TmAu_2$ shows very complex (H, T) magnetic phase diagrams: up to five different phases exist in a magnetic field applied along the [100] orthorhombic axis, i.e. the quadrupolar axis of easy magnetization [6]. This complexity seems to originate not only from anisotropy and bilinear magnetic coupling, but probably reflects the field competition between quadrupolar and antiferromagnetic order parameters. Indeed, in a quadrupolarly ordered state, the highest magnetic susceptibility, thus the lowest energy, is obtained for a magnetic field along the quadrupoles axis (i.e. the z-axis along which $\langle 3J_z^2 - J(J+1)\rangle$ is maximum). On the contrary, in a collinear antiferromagnet, the maximum of the susceptibility is obtained for magnetic moments and, therefore, a quadrupoles axis perpendicular to the field.

To investigate this original coexistence between quadrupolar and antiferromagnetic order, we have undertaken an extensive neutron diffraction study of the different phases stabilized for a field along [100]. In this paper, we first briefly recall the [100] magnetic phase diagram, the experimental conditions (section 2) and, second, present the different determinations (section 3).

2. The $TmAu_2$ system

$TmAu_2$ belongs to the family of heavy rare-earth intermetallics, which crystallize within the $MoSi_2$-type body-centred tetragonal structure, the alloyed metal being Ag or Au. The RAg_2 and RAu_2 series were systematically studied 30 years ago by Atoji by powder neutron diffraction ([7] and references therein). The compounds are antiferromagnetic. They order at T_N in incommensurate structures, then move through a first-order transition to a commensurate state characterized by the propagation vector [1/2 1/2 0], which corresponds to the X point in the Brillouin zone (figure 1). This first-order transition between a high-temperature incommensurate structure to a low-temperature commensurate one is quite usual in magnetic compounds. It constitutes one of the main ways for the magnetic system to minimize its energy and 0 K entropy, another one being the squaring-up of the incommensurate magnetic structure. Powder neutron diffraction spectra essentially inform on the modulus of the magnetic propagation vector; ambiguities can remain on its exact direction. This is the case here for the

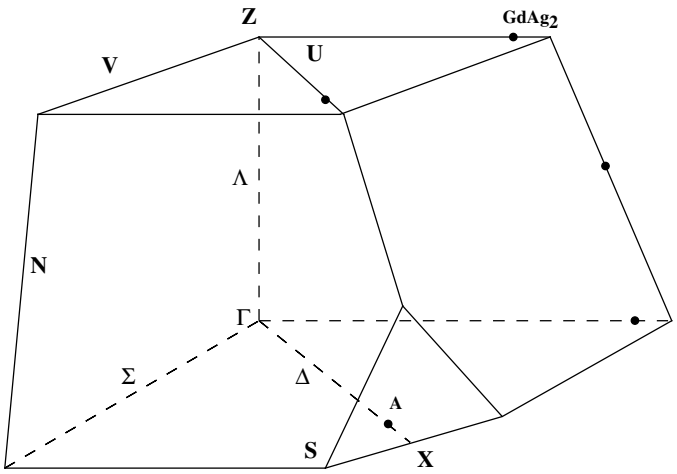

Figure 1. The Brillouin zone of the body-centred tetragonal structure of RAg_2 and RAu_2 compounds. Black dots are the intercepts of high-symmetry directions with the sphere having as radius the modulus of the propagation vector determined by powder neutron diffraction; dot A corresponds to the determinations by Atoji, dot $GdAg_2$ to the best fit of neutron intensities in $GdAg_2$.

incommensurate structure: in figure 1, the dots correspond to the intersection points of high symmetry directions in the Brillouin zone and the sphere, the radius of which has the same modulus as the high-temperature propagation vector. In $Tb^{3+}-Tm^{3+}$ compounds with silver and gold, Atoji analysed all the structures immediately below T_N using the incommensurate propagation vector close to the X point (dot A along ΓX in figure 1). The vicinity of the two propagation vectors, commensurate and incommensurate, very likely corresponds to a small change in the strength of the bilinear exchange integral, $J(Q)$, and the analysis of Atoji is quite logical from an energetical point of view. The situation of $GdAg_2$, also studied by powder neutron diffraction using a small wavelength, is different: the modulus of the propagation vector is the same as in the Atoji studies, but the fit of the neutron intensities led us to conclude to an incommensurate propagation vector along the V-edge of the Brillouin zone (see figure 1) [8]. In spite of their very different orientations, these two incommensurate vectors will be encountered, among others, in $TmAu_2$, which could indicate a similar Fourier transform $J(Q)$ of the exchange couplings.

Figure 2 gives the magnetic phase diagram determined by isothermal and isofield magnetization processes in a field applied along the [100] quadrupolar axis [6]. The magnetization processes can be marked by clear magnetization jumps, but in general the anomalies are very delicate and observable essentially on the derivatives of the magnetization. The spontaneous phase I, below T_N, is observed to be stable down to 0.1 K. If incommensurate, as is the rule in RAg_2 and RAu_2, this should imply a squaring-up of the magnetic structure at low temperature. Close to T_N, in fields larger than 4.2 kOe, phase I is replaced by the triangle-shaped phase II. At low temperature and in magnetic fields higher than 2.5 kOe, phase I vanishes in favour of phase III, characterized by a ferromagnetic component of 1.6 μ_B along the field direction. Phase III is separated from the paramagnetic phase by phase IV. This latter, very narrow field, persists down to 0.1 K. At low temperature, phase V inserts itself between phases III and IV; it is very narrow in field and not easily defined.

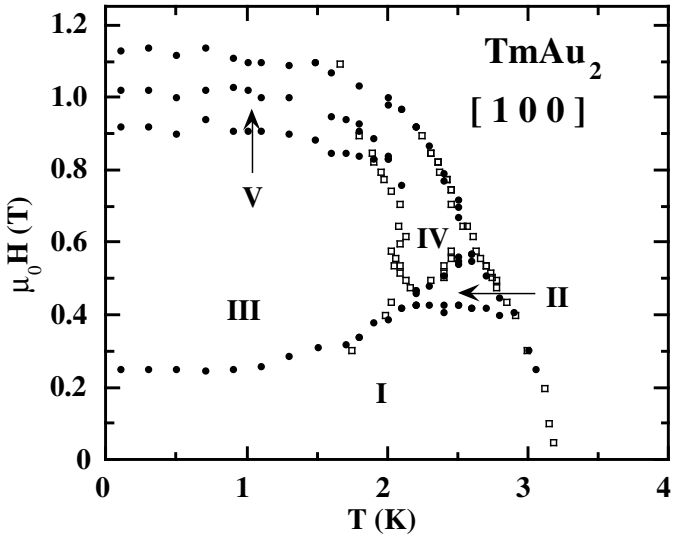

Figure 2. Magnetic phase diagram along the [100] twofold direction of $TmAu_2$ after [6] (open squares: from temperature variation of the magnetization in constant magnetic fields; black dots: from field variations at constant temperatures); phases are labelled in coherence with the text.

The transition line between antiferromagnetism and polarized paramagnetism has the usual aspect for an antiferromagnet and the small low-temperature coordinate, 11 kOe, agrees with the weakness of the antiferromagnetic interactions characterized by $T_N = 3.1$ K. The lines between phases I and III, or II and IV, with their unusual positive slope in an antiferromagnetic (H, T) phase diagram, may result from different behaviour under field of the magnetic moments system and the quadrupoles one, as mentioned in section 1. In order to be confirmed, this qualitative analysis proposed by Morin *et al* [6] requires, first, a complete determination of the structure associated with each of the different phases, second, a quantitative analysis by numerical calculations considering the various couplings, as done for the complex magnetic properties of cubic NdZn, also ruled by quadrupolar and magnetic interactions [9].

3. Neutron diffraction results

All the neutron elastic scattering studies presented here have been performed on the single crystals previously used in the magnetization studies. They were cut along the c-axis or the a-axis of the tetragonal $MoSi_2$-type structure from an ingot grown by the Czochralski method. Samples were annealed at 1000°C for a week under ultra-high vacuum. The D15 spectrometer at ILL high-flux reactor in Grenoble was used with and without the presence of a vertical magnetic field; the wavelength was set at 0.1174 nm.

3.1. The quadrupolar phase

The quadrupolar structure was studied within the conditions of a vertical a-axis. In order to improve the experimental accurracy with respect to the lattice distortion, nuclear reflections were scanned at high 2θ angles, in particular the [5 0 3] one. Examples of such [QH 0 3] scans for QH ranging from 4.95 to 5.05, in the absence of magnetic field, are given in figure 3. The single peak observed at 10 K, in the tetragonal phase, splits into two components below T_Q due

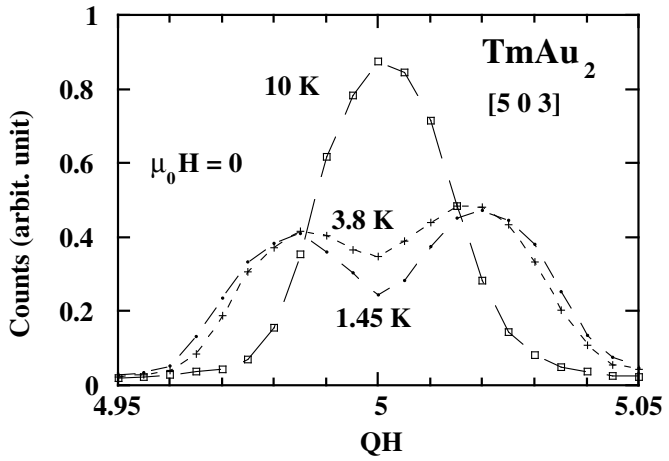

Figure 3. QH scans of the (503) nuclear reflection in null magnetic field at the temperatures indicated; counts are compared to the monitor value.

to the partition of the sample into two families of orthorhombic domains. These components are of similar amplitude, which indicates an approximate equipartition of the sample. No anomaly reveals the entrance into the antiferromagnetic phase at T_N. From these results of figure 3, it is not possible to deduce the sign of the symmetry lowering. Only the absolute value of the relative change in the lattice parameter a, $|a_{or} - a'_{or}|/a = 4 \times 10^{-3}$, can be achieved at low temperature.

As previously evoked, applying a magnetic field rises a conflict between quadrupoles and magnetic moments: it is very likely that the spontaneous phase I has the axis common for quadrupoles and magnetic moments perpendicular to the field, whereas in phases III and IV, as well as in the paramagnetic orthorhombic one, this common axis is parallel to the field. Then a field value of 0.65 T allows us to study the sample with a vertical a-axis, from the tetragonal phase, say 10 K, down to the lowest temperature, without a huge modification of the sample's magnetostriction and damage for the gluing point. Some examples of [5 0 3] scans are given in figure 4. A systematic shift of the peak is observed toward the low value of QH. This is the signature of an increase of the corresponding lattice parameter in the equatorial plane (i.e. of the a value perpendicular to the field). Along the vertical quadrupolar axis the cell contracts itself; the symmetry-lowering strain is negative in agreement with the determination by means of parastriction [6]. Entering the antiferromagnetic phases IV and III, at 2.55 and 2.1 K (figure 5), is not revealed in our experimental conditions by any specific anomaly. This may be understood by the fact that the magnetic interactions are not able to significantly alter the quadrupolar state.

3.2. The spontaneous structure in phase I

The study in null field was realized in a ILL orange cryostat with the tetragonal c-axis vertical. The orientation matrix used at 1.4 K is the same as used at 10 K, because it is impossible to work on a single family of magnetic twins, as they are not separated enough from the other one. The angular variation of the rotation around the vertical axis between the two neighbouring peaks, $\Delta\omega$, will be reduced when increasing the diffraction vector and measuring the integrated intensities will mix the contributions of the domains.

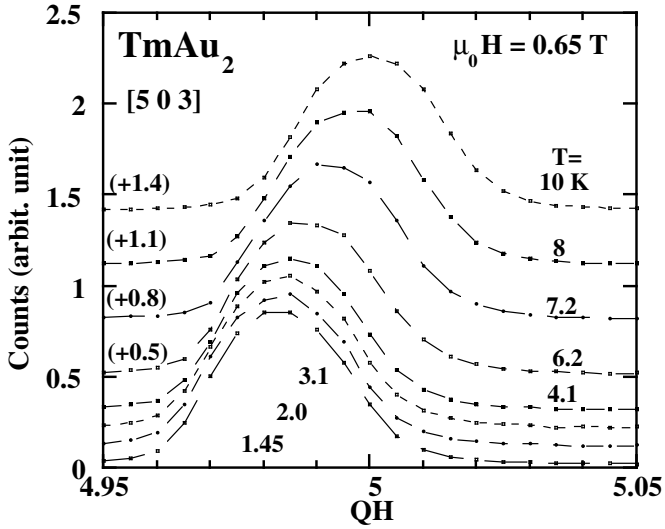

Figure 4. QH scans across the (503) nuclear reflection in the different phases of $TmAu_2$; the magnetic field of 0.65 T is applied vertical, parallel to a twofold orthorhombic axis; counts are compared to the monitor value.

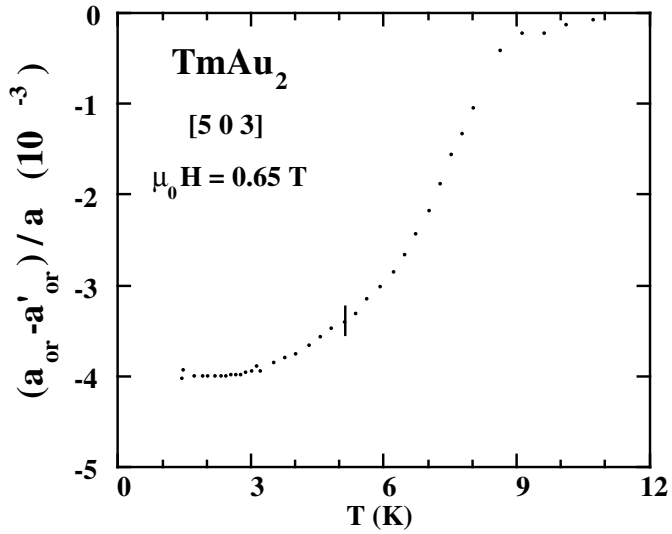

Figure 5. Temperature variation of the relative change of lattice parameter in the orthorhombic range of $TmAu_2$; a is the tetragonal lattice parameter, a_{or} and a'_{or} are the two orthorhombic parameters, the first one corresponds to the quadrupolar axis, which is the direction of easy magnetization. The bar is indicative of the uncertainties in the measurements.

The search for magnetic peaks was done by various scans across the Brillouin zone. Figure 6 shows the results of transverse scans in the surrounding of the origin node. The magnetic nature of these eight satellites was checked through their temperature dependence: they vanish above $T_N = 3.1$ K. They can be indexed with $q = (0.4\ 0.4\ 0)\pm(\tau\ -\tau\ 0)$ with $\tau = 0.040(1)$. Note the value of τ is much larger than what could be ascribed to the lattice distortion in

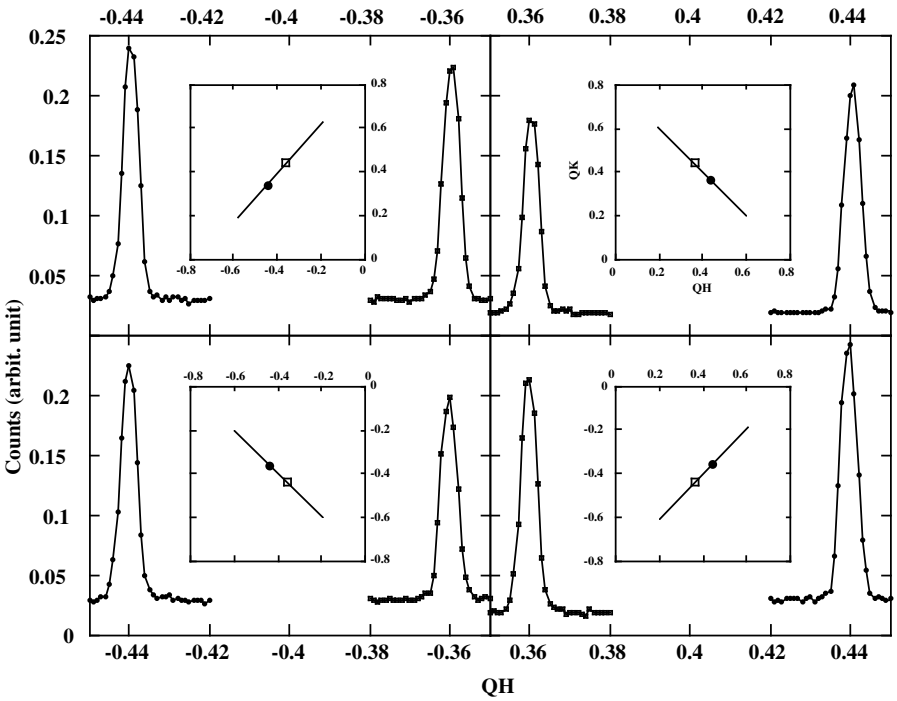

Figure 6. Transverse scans of the magnetic satellites of the origin node in the tetragonal reciprocal cell measured at 1.4 K in the spontaneous phase I of $TmAu_2$; counts are compared to the monitor value. The insets describe the associated paths in the basal reciprocal plane, the open squares and full dots referring to the maximum of the scans.

case of a wave vector on the diagonal of the basal plane. Within the orthorhombic reciprocal lattice, the observed satellites are then related to an off-diagonal wave vector. Each of the two quadrupolar orthorhombic domains should then decompose into two k magnetic domains. Taking account of $-\boldsymbol{k}$ in addition to $\boldsymbol{k}$, this gives rise to a total of eight magnetic satellites. In the following we will refer to the two families of orthorhombic domains by $(+\tau\ -\ \tau)$ and $(-\tau\ +\ \tau)$, each of these covering two k magnetic domains. The positions of the maximum for the eight satellites are given in the insets of figure 6, where the symbols, full dot or open square, refer to the associated transverse scan of the same figure. In all magnetic domains, the propagation vector $\boldsymbol{k}$ and its Fourier component $\boldsymbol{m_k}$ have the same respective orientation. The fact that the counts, normalized to the monitor value, are similar for the peaks originating from the two orthorhombic domains is additional evidence of their almost equipartition. The wave vector found for $TmAu_2$ phase I is then close to the incommensurate propagation vector observed in RAg_2 and RAu_2 by Atoji, for whom the very small value of τ was impossible to detect from powder neutron diffraction spectra.

Similar collects were done for magnetic satellites of the Brillouin zone centres [200], [020], [110]. In the latter case, the intensities of the eight satellites are similar for the same symmetry and equipartition reasons as around the reciprocal lattice origin. Around each of the other two nodes (figure 7), only the 4 satellites associated with one family of domains can be easily observed owing to the angle between the diffraction vectors and the Fourier component. To explain such a difference, this angle should be close to 90° for one family and to 0° for the other. This implies that in the orthorhombic domains, $(-\tau\ +\ \tau)$ or $(+\tau\ -\ \tau)$, the magnetic

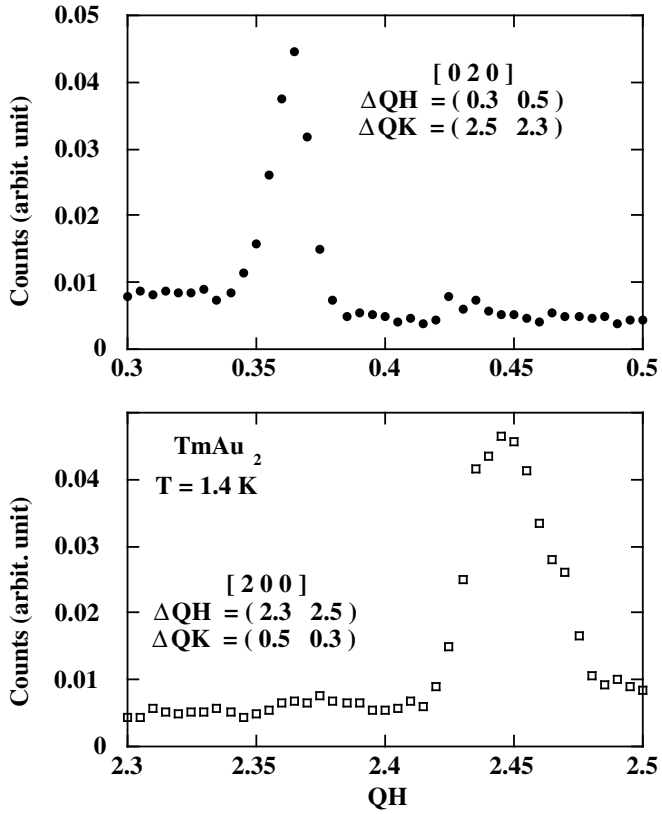

Figure 7. Equivalent transverse scans around the (020) and (200) Brillouin Zone centres in the tetragonal reciprocal lattice measured at 1.4 K in the spontaneous modulated phase I of $TmAu_2$; counts are compared to the monitor value.

moments are respectively aligned along [1 0 0] or [0 1 0].This is consistent with the magnetic measurements which show that the [1 0 0] axis is the easy direction, the axis along which the *a* lattice parameter decreases being further privileged within the orthorhombic phase [6].

For a more accurate determination of this magnetic structure, a collection of magnetic and nuclear reflections was measured under zero magnetic field at $T = 1.6$ K. These integrated intensities have been compared with the calculation based on the single *k* model (inset of figure 8), which Fourier description reads as:

$$\boldsymbol{k} = (0.44\,0.36\,0) \qquad \boldsymbol{m_k} = [0\,m\,0].$$

The phase shift of the magnetic wave is undetermined; the sketch of figure 8 arbitrarily corresponds to a phase which maximizes the average of the squared magnetic moment and is thus associated with the minimum exchange energy. As already mentioned, four domains have to be considered, which in the calculation brings in four proportion parameters, p_j, in addition to the moment amplitude m and the apparatus constant C_{app}. The intensity of a magnetic reflection is:

$$I_{magn}(hkl) = C_{app} \sum_{j=1,4} p_j \left(C_{magn} f(\sin\theta/\lambda) m \sin([hkl], \boldsymbol{m_{kj}})\right)^2.$$

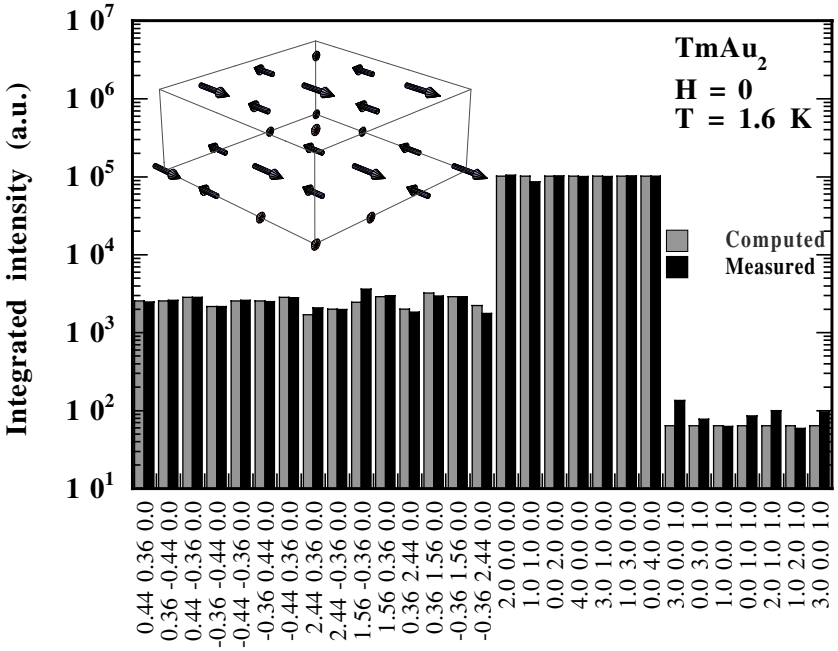

Figure 8. Comparison between measured and computed neutron diffraction reflections within $TmAu_2$ magnetic phase I. The intensities scale is logarithmic in order to display magnetic, strong and weak nuclear reflections on a unique graph. The inset shows the used model of magnetic structure, here simplified using (0.4 0.4 0) as wave vector, instead of (0.36 0.44 0).

Where $C_{magn} = 0.27 \times 10^{-12}$ cm is the magnetic scattering constant and $f(\sin\theta/\lambda)$ is the magnetic factor for Tm^{3+} [10].

The apparatus constant C_{app} is defined for a single crystallographic cell of the $MoSi_2$ type structure, including then two Tm^{3+} ions. This is the reason for the absence of a factor 1/2 in the definition of the magnetic scattering amplitude, since it cancels with the double contribution of the Tm^{3+} ions. For this cell, including two Tm and four Au, the intensity of a nuclear reflection is:

$$I_N(hkl) = C_{app}|F(hkl)|^2 = c_{app}2\left[b_{Tm} + 2b_{Au}\cos\left(\frac{2\pi}{3}l\right)\right]^2 [1 + \cos\pi(h + k + l)].$$

Where $b_{Tm} = 0.707 \times 10^{-12}$ cm and $b_{Au} = 0.763 \times 10^{-12}$ cm are respectively the thulium and gold coherent scattering lengths [11]. Their values are such that the intensity for the weak reflections almost cancels. In the quantitative description of the scattered intensities, one is then faced with a scaling problem. Indeed, the average value of the magnetic reflections is much higher than the one of a weak nuclear reflection but, also, far below the value of a strong nuclear one. The apparatus constant cannot then be unambiguously defined after the weak nor after the strong nuclear reflections. To get an accurate value for the ordered magnetic moment m, one would need a detailed study of the extinction phenomena which is outside our present scope. The result of the refinement then gives a rather wide interval for m, between the minimum, for C_{app} based on weak nuclear reflections and the maximum, for C_{app} based on strong nuclear reflections (see figure 8). Using C_{app} or m as free parameter, all the refinements correspond to the same average error of 10.6%. One then obtains: $5.7\ \mu_B < m < 6.7\mu_B$. This value range corresponds to about twice Atoji's determination [7].

However, this is consistent with the magnetization measurements for a field along the easy [100] direction. Indeed, from a simple mean-field approach, an estimate of the ordered moment amplitude can be deduced from the intercept between the average slope in the antiferromagnetic range, which represent the exchange line, and the paramagnetic curve. In such conditions one obtains 5.5 μ_B at $T = 1.6$ K [6].

The search for magnetic third-order harmonics in the 1.4–1.5 K thermal range produced no results: no squaring-up of the modulated structure occurs down to $T_N/2$; this does not rule out the occurrence of such phenomena in $TmAu_2$, but answering this question would require an additional study using a dilution refrigerator. The temperature variation of the amplitude of the magnetic satellite of the origin measured by transverse scans is given in figure 9 (black dots, right scale). The temperature dependence of the propagation vector was also studied in order to observe the possible locking on commensurate values. The τ value varies slightly and monotonously in all the accessible temperature range without any significant plateau (figure 9, open squares, left scale), the 0 K extrapolated value does not exhibit any specific feature.

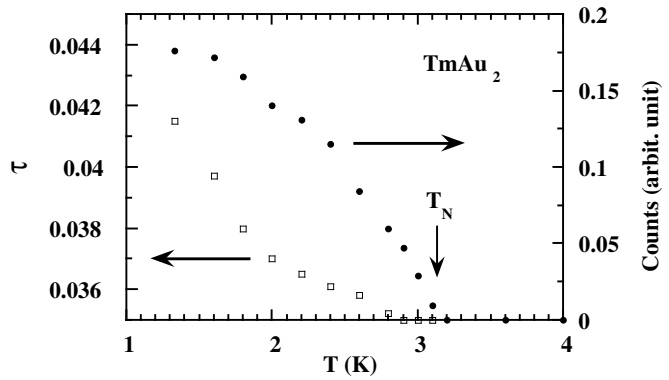

Figure 9. Black dots and right scale; temperature variation in phase I of $TmAu_2$ of the amplitude of the magnetic satellite of the origin, measured by transverse scans and normalized to the monitor. Open squares and left scale; temperature variation of the τ component of the propagation vector $(0.4\ 0.4\ 0)\pm(\tau\ -\tau\ 0)$ describing the modulated structure in phase I of $TmAu_2$.

3.3. The magnetic structure in phase III

The sample was oriented with the [0 1 0] twofold axis vertical in order to be parallel to the applied magnetic field as in the study of the quadrupolar state. At 1.3 K, the field was raised from zero in order to follow the field dependence of the propagation vector in the spontaneous phase I by means of $(Q\,H,\ Q\ K)$ transverse scans; their amplitude starts to decrease at 0.28 T and falls to the background level at 0.36 T in agreement with the transition line determined by magnetic measurements.

In order to find the new propagation vector in this phase III, the magnetic field was fixed at 0.5 T and the temperature at 1.3 K; scans were collected along all the principal directions of the Brillouin zone accessible within the experimental conditions. A magnetic peak was observed in (1/3 0 1), which is very close to the (0.362 0 1) propagation vector describing the incommensurate structure in $GdAg_2$ [8]. Then the change of propagation vector is quite important and the somewhat exotic situation of $GdAg_2$ among the RAg_2 and RAu_2 compounds is here indirectly confirmed.

Such a wave vector is typical of an Ising-like constant amplitude magnetic structure carrying a ferromagnetic component. In order to avoid the interference of wave vectors with unfavourable $J(Q)$ couplings, the system uses this method to achieve a square structure which calls into play only two wave vectors, (1/3 0 1) and (0 0 0). All odd harmonics of (1/3 0 0) are either equivalent to itself or equivalent to (0 0 0). The magnetic moments being parallel or antiparallel to the field, the Fourier description of the structure restricts to:

$$\boldsymbol{k}_0 = (0\,0\,0) \qquad \boldsymbol{m}\boldsymbol{k}_0 = [0\,m/3\,0] \qquad \boldsymbol{k}_1 = (1/3\,0\,1) \qquad \boldsymbol{m}\boldsymbol{k}_1 = [0\ -4m/3\,0].$$

To ensure a constant amplitude for the magnetic moments, the phase shift for the antiferromagnetic component has to be fixed at zero here (in case of a cosine description with the origin at a Tm site). This structure, represented in the inset of figure 10, consists for the moments, parallel to [0 1 0], in a sequence $(- + + - ++)$ along the [1 0 0] direction. A collect of integrated intensities, at $\mu_0 H = 0.5\,T$ and $T = 1.3$ K, was done in order to confirm this model and to determine the magnetic moment. Here also, the difference in magnitude between magnetic, weak and strong nuclear reflections is such that only an interval can be defined for the m value. In the calculation for refining the structure, a single domain has to be taken into account, the expression for an antiferromagnetic reflection being then:

$$I_{magn}(hkl) = C_{app}\left(C_{magn}\,f(\sin\theta/\lambda)\frac{4m}{3}\sin([hkl], \boldsymbol{m}_{k1})\right)^2.$$

Figure 10 shows the result of the refinement with C_{app} computed from strong nuclear reflections. The average error is 11.3%. The interval for the moment amplitude m is: $3.5\ \mu_B < m < 6.2\ \mu_B$, the associated magnetization along [0 1 0] being then between 1.2 and 2.1 μ_B. Both intervals are consistent with the values deduced from magnetization measurements, 5.5 μ_B for m (see section 3.2) and, at $T = 1.6$ K and $\mu_0 H = 0.5\,T$, 2 μ_B per Tm for the measured magnetization [6].

3.4. Field and temperature variations

In order to determine the magnetic structures in phases II, IV and V or, at least, the propagation vectors and the direction of the Fourier component, isofield and isothermal variations were used according to the shape and position of these phases in the (*H–T*) diagram. In the case of phase IV, the field was kept constant at 0.65 T and the temperature increased from 1.3 K. Figure 11 gives some examples of scans at characteristic temperatures; in phase III around 1.9 K, the maximum amplitude of the scans has strongly decreased in comparison with the 1.3 K value. At higher temperatures, around 2.2 K, in the thermal range of phase IV, the maximum observed is shifted to the position [0.295 0 1] and is clearly reduced; this agrees with an increased temperature and also with the magnetic measurements, which indicate a larger ferromagnetic component in phase IV than in phase III (see for instance the thermal variation in 0.8 T in figure 7 in [6]). In phase IV, the structure is then most probably of Ising-type, similar to the one of phase III. Nevertheless, it introduces incommensurate aspects, leaving the constant modulus for the benefit, at higher temperature and field, of a more favourable antiferromagnetic $J(Q)$ coupling and a larger magnetic susceptibility.

Measurements at 1.4 K for various field values were performed while moving from phase III (field lower than 0.9 T) up to the paramagnetic state (field larger than 1.1 T) through phases V and IV (figure 12). Longitudinal scans around (1/3 0 1) revealed in phase V a new propagation vector, (0.311 0 1), in coexistence with the (1/3 0 1) one. This wave vector is intermediate between (1/3 0 1) in phase III and (0.295 0 1) in phase IV. As phase IV, phase V is probably a compromise between phase III and the polarized paramagnetic state. It clearly appears from the magnetization measurements that the Ising-like structure of phase III has

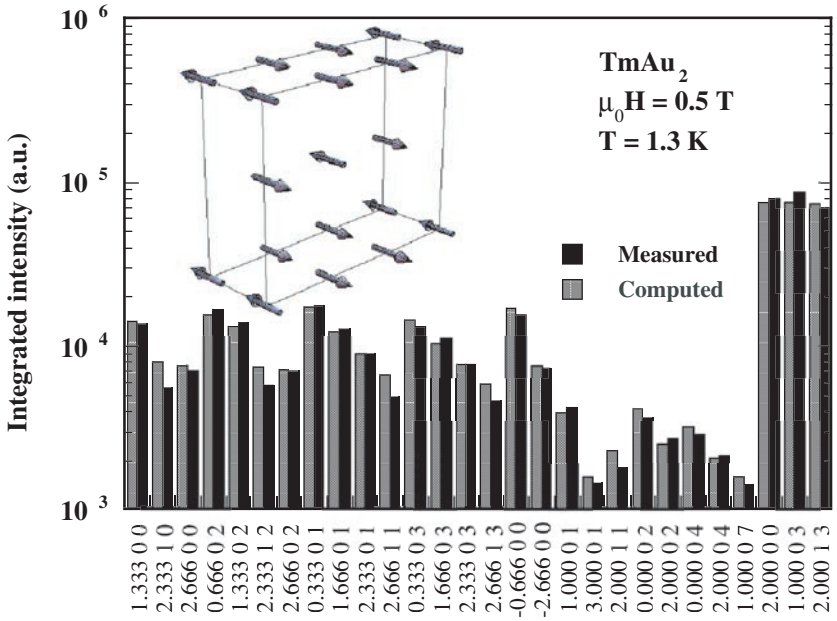

Figure 10. Comparison between measured and computed neutron diffraction reflections within $TmAu_2$ magnetic phase III. The intensities scale is logarithmic in order to display magnetic, strong and weak nuclear reflections on a unique graph. The inset shows the used model of Ising-like magnetic structure, mixing one (1/3 0 1) antiferromagnetic component with a ferromagnetic one.

a small magnetic susceptibility. This is easy to understand since, for this constant modulus structure, the exchange field is large on all Tm sites and the influence of the applied field relatively small. As the field is increased, the system finds it more convenient to call into play new incommensurate wave vectors, thus creating sites of low-exchange field, which are then more liable to respond to the magnetic field. From reflections measured for different $\boldsymbol{Q}$ vectors, the antiferromagnetic component is also found parallel to the magnetic field in phases IV and V. In addition to an insignificant temperature dependence of the propagation vectors, we have noted the coexistence of the different phases in a given field range (figure 12). This could result from crystalline defects as well as from the close values of the energies of the different phases in presence.

Phase II was studied in a constant magnetic field of 0.48 T using longitudinal (QH 0 1) scans in decreasing temperature from the polarized paramagnetic phase (figure 13). Phase II is characterized by a (0.14 0 1) wave vector which appears at 2.68 K, i.e. immediately below the transition temperature in full agreement with the magnetization data. At $T = 2.35$ K, the (0.295 0 1) wave vector, characteristic of phase IV, appears in coexistence with the (0.14 0 1) one. The latter has disappeared at 2.23 K whereas the (1/3 0 1) wave vector of phase III starts coming out of the background. These observations confirm the complex magnetic phase diagram determined by magnetic measurements and, in particular the existence of the phase II characterized by the (0.14 0 1) wave vector. From reflections measured for different $\boldsymbol{Q}$ vectors equivalent to (0.14 0 1), we were able to conclude that the antiferromagnetic component is also parallel to the magnetic field. The direction of the quadrupolar axis in phase II is then dubious. The transition line, which separates phase I from phase III (figure 2) and which

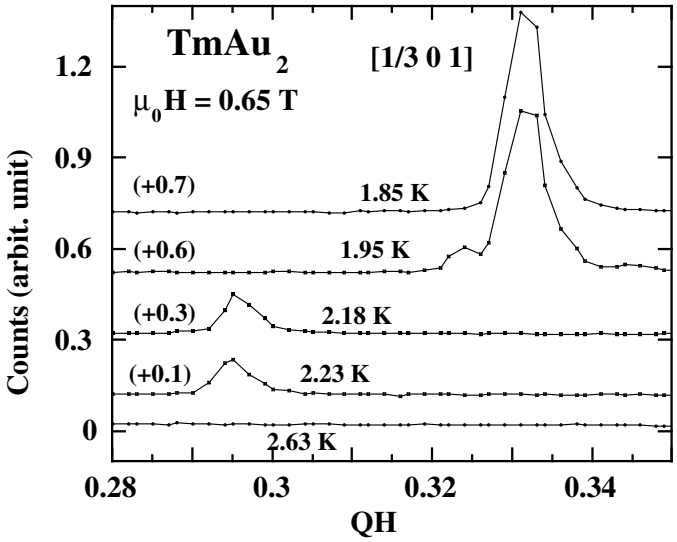

Figure 11. Longitudinal QH scans across the (1/3 0 1) reflection collected in a magnetic field of 0.65 T at different temperatures: in phase III (1.85, 1.95 K), in phase IV (2.18, 2.23 K) and in the paramagnetic range (2.63 K); counts are compared to the monitor value and translated by the values indicated.

corresponds to the rotation of the quadrupolar axis from perpendicular to parallel with the field, seems to find its natural continuation in the line between phases II and IV. Therefore, one would expect that in phase II, unlike the antiferromagnetic moments, the quadrupolar axis is still perpendicular to the field. This is difficult to understand since the magnetic anisotropy is clearly in favour of the quadrupolar axis [6]. The wave vector of phase II also raises a contradiction with this continuity hypothesis for the quadrupolar flip-line. Indeed, it belongs to the same family [α 0 1] as the ones of phase III, V and IV, which are all located above the incriminated line of the (H, T) phase diagram. It is then not possible, at this state of the investigation to solve this question and additional measurements are needed, as for example, magnetostriction measurements across phases I, II and IV.

4. Conclusion

As a continuation to the macroscopic investigations, this neutron scattering study of $TmAu_2$ has brought new information regarding the antiferromagnetism which may develop in a ferroquadrupolarly ordered state. Part of the appearance of the (H, T) phase diagram can be directly ascribed to the coexistence of two order parameters of different natures and then of different responses to the field. Unlike the magnetic moments, the quadrupolar components do not couple directly with the field but are active in determining the magnetic anisotropy. In the present case, the quadrupolar order introduces a difference in the magnetic response of Tm^{3+} along the two twofold axis of the initially tetragonal system. This then defines the direction of the moments in the spontaneous phase I, the wave vector of the antiferromagnetic structure being the result of the particular indirect exchange couplings of this system. Applying a field along [0 1 0], first selects the domains of maximum susceptibility with moments perpendicular to the field, as usual in a collinear antiferromagnet. However, here this also results in the selection of one of the two orthorhombic domains, the one for which the $\langle O_2^2 \rangle$ order parameter

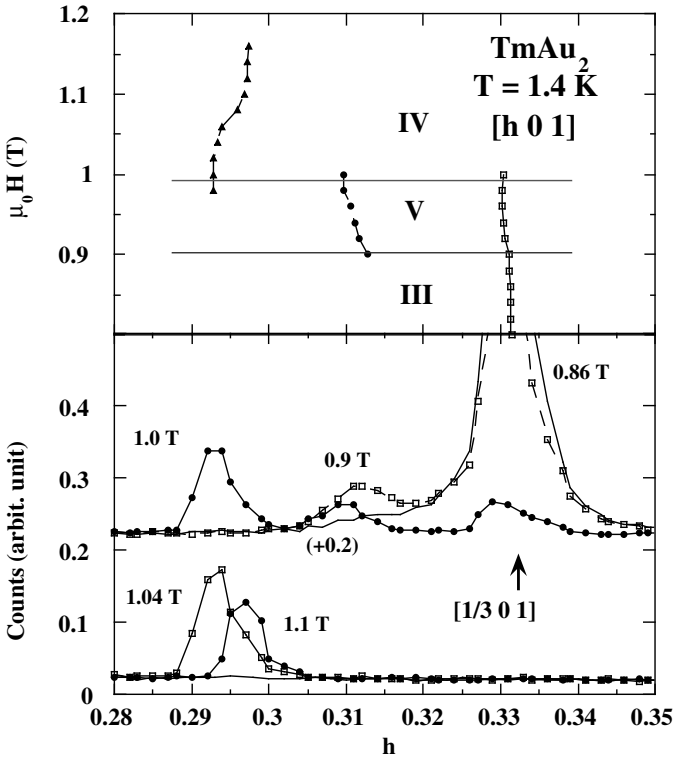

Figure 12. Upper part; field dependence across phases III, V and IV, of the antiferromagnetic wave vector, as deduced from longitudinal scans around (1/3 0 1) at 1.4 K. Lower part; some of the associated scans for different magnetic fields. Note the interference of a new propagation vector, (0.311 0 1), characteristic of phase V where it coexists with (1/3 0 1). The counts are normalized to the monitor value, the 1 , 0.9 and 0.86 T curves being shifted by +0.2. The flat full line in the lower part of the figure corresponds to the scan collected in a field of 1.2 T, i.e. in the paramagnetic range.

is positive. Further increasing the field, the transverse susceptibility of the spontaneous phase can no longer compete with a solution in which at least part of the moments are parallel with the field. This is the case of the structures associated with phases III, V and IV. But due to the quadrupolar order induced anisotropy, the quadrupolar axis has to also change, that is the selected orthorhombic domain differs from the one of phase I under field and corresponds with a negative $\langle O_2^2 \rangle$ order parameter. The transition between phase I and III is not then a simple spin-flip one, the quadrupolar order parameter changing its sign simultaneously. Above this line, the magnetic structures are all of Ising-type, the magnetic moments being parallel or antiparallel to the field, the Fourier description including at least one antiferromagnetic component in addition to the ferromagnetic one. There are numerous antiferromagnetic wave vectors observed within the magnetically ordered states of $TmAu_2$, (0.44 0.36 0) for phase I, (1/3 0 1) for phase III, (0.311 0 1) and (1/3 0 1) for phase V, (0.295 0 1) for phase V and (0.14 0 1) for phase II. This indicates a rather degenerated maximum for the $J(Q)$ Fourier transform of the indirect exchange coupling, with two remote regions of almost equivalent coupling, that is the surroundings of point A- and the V-edge of figure 1. Except for the transition between phases I and III which correspond to the appearance of a net ferromagnetic component associated with a quadrupoles and spin reorientation, the other transitions result from subtle compromises

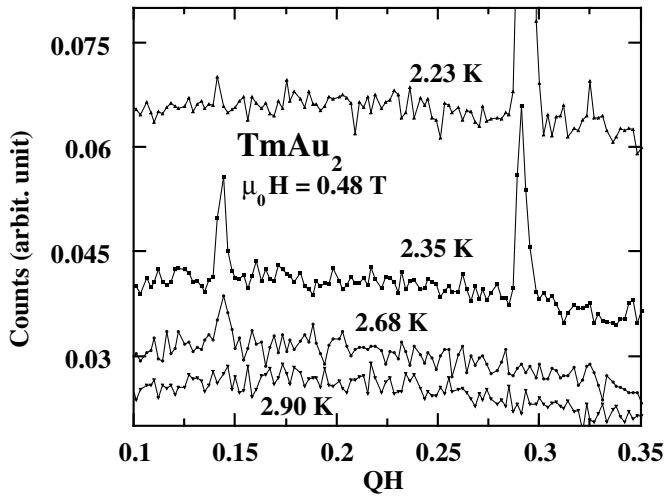

Figure 13. Longitudinal scans (QH 0 1) in a constant magnetic field of 0.48 T for decreasing temperature; the full line is collected at 2.90 K in the paramagnetic state, the other two ones are vertically shifted by 0.005 and 0.015, respectively. The counts are normalized to the monitor value. Note the new propagation vector, (0.145 0 1), existing immediately below the antiferromagnetic transition and characteristic of phase II.

involving a rather flat $J(Q)$ curve along the V-edge. The structure of phase III ensures constant magnetic moment amplitude and a net ferromagnetic component. This phase is of low entropy and magnetic susceptibility; as the field or temperature are increased, it is replaced by structures with slightly different, incommensurate, wave vectors, namely phases V and IV. More delicate is the discussion of the phase II, for which the quadrupoles orientation is unknown and the transition line with phase IV of surprisingly large positive slope in the (H, T) phase diagram. This may be solved by additional macroscopic measurements, in particular, magnetostriction within the magnetically-ordered state.

A challenging perspective and next step in the study of $TmAu_2$ is the quantitative or semiquantitative description of the coexistence between quadrupolar and antiferromagnetic order. This may be achieved using the proven microscopic models of 4f magnetism, including the crystal field Hamiltonian, the Zeeman and the magnetoelastic terms, with a molecular field treatment of both bilinear exchange and quadrupolar pair interactions.

References

[1] Gehring G and Gehring K 1975 *Rep. Prog. Phys.* **38** 1
[2] Morin P and Schmitt D 1990 *Ferromagnetic materials* 5 eds K H J Buschow and E P Wohlfarth (Amsterdam: North-Holland) 1
[3] Stevens K H W 1952 *Proc. Phys. Soc.* A **65** 209
[4] Morin P and Rouchy J 1993 *Phys. Rev.* **48** 256
[5] Kosaka M, Onodera H, Ohoyama K, Ohashi M, Yamaguchi Y, Nakamura S, Goto T, Kobayashi H and Ikeda S 1998 *Phys. Rev.* **58** 6339
[6] Morin P, Kazei Z and Lejay P 1999 *J. Phys.: Condens. Matter* **11** 1305
[7] Atoji M 1970 *J. Chem. Phys.* **52** 6434
[8] Gignoux D, Morin P and Schmitt D 1991 *J. Magn. Magn. Mater.* **102** 33
[9] Amara M and Morin P 1996 *Physica* B **222** 61–72
[10] Stassis C, Deckman H W, Harmon B N, Desclaux J P and Freeman A J 1977 *Phys. Rev.* B **15** 369
[11] *Neuton Scattering Lengths* 1992 *Neutron News* p 29